Enhancing mechanical durability of icephobic surfaces by introducing autonomous self-healing function

Yizhi Zhuo, Verner Håkonsen, Zhiwei He, Senbo Xiao, Jianying He and Zhiliang Zhang**

NTNU Nanomechanical Lab, Department of Structural Engineering, Norwegian University of Science and Technology (NTNU), Trondheim 7491, Norway.

Corresponding Author

*E-mail: jianying.he@ntnu.no; zhiliang.zhang@ntnu.no

ABSTRACT: Ice accretion presents a severe risk for human safety. Despite great efforts for developing icephobic surfaces (the surface with an ice adhesion strength below 100 kPa) have been devoted, expanding the lifetime of state-of-the-art icephobic surfaces still remains as a critical unsolved issue. Herein, a novel icephobic material is designed by integrating interpenetrating polymer network (IPN) into autonomous self-healing elastomer, and applied in anti-icing for enhancing mechanical durability. The molecular structure, surface morphology, mechanical properties and durable icephobicity of the material were studied. The creep behaviours of the new icephobic material, which were absent in most relevant studies on self-healing materials, were also investigated in this work. Significantly, the material showed great potentials for anti-icing applications with an ultralow ice adhesion strength of 6.0±0.9 kPa, outperforming many other icephobic surfaces. The material also exhibited extraordinary durability, showing a very low long-term ice adhesion strength of ~12.2 kPa after 50 icing/deicing cycles. Most importantly, the material was able to demonstrate self-healing from mechanical damages in a sufficiently short time, which shed light on the longevity of icephobic surface in practical applications.

KEYWORDS: self-healing, ice adhesion strength, creep, anti-icing, icephobicity

INTRODUCTION

The accumulation of ice and snow has a severe effect on infrastructures and transportations, including airplane, marine structures, wind turbines, power line and many others.[1-2] Traditional methods of ice removal, for instances by active heating or using anti-freeze fluids were proven to be energy-intensive or can yield unsolvable environmental problems. In the recent years, many researches have been focusing on developing environmental friendly passive icephobic surfaces that can repel the incoming cold water droplets,[3-6] delay ice nucleation,[7-9] and reduce ice adhesion strength.[10-17] Since ice formation on the surface was proven to be inevitable under harsh environment, numbers of studies have been devoted to develop surfaces with low ice adhesion strength (<100 kPa).[18-25] To date, one of the most famous icephobic surfaces, the slippery liquid-infused porous surfaces (SLIPS), had achieved ultralow ice adhesion strengths of ~15,[24] 1.7,[26] and 0.4 kPa,[27] in different studies. The icephobicity of the SLIPS was enabled by the existence of lubricating oil film at the ice-contacting interface, inspired by the Nepenthes pitcher plant.[23] However, the icephobicity for such surfaces degrades gradually along with the depletion of the lubricant via evaporation or removing away by water droplets or forming ice.[11] In order to enhance durability of such surfaces, bioinspired solid organogel materials with a regenerable sacrificial alkane surface layer had been prepared, the ice adhesion strength of which (~68.8 kPa) remains almost unchanged after 20 icing/deicing cycles.[28] Unfortunately, such ice adhesion strength value was not low enough for passive deicing. Another key strategy to achieve ultralow ice adhesion strength is to use low-modulus materials.[11, 29] This type of icephobic surfaces demonstrated ultralow ice adhesion strength of 0.2,[11] and 5.2 kPa.[29] The low ice adhesion strength on these low-modulus surfaces was attributed to the voids formed at the interface, which can serve as fracture initiators

favouring adhesive failure under shearing forces.[11, 29-31] Most recently, our group presented a novel icephobicity mechanism of crack initiators, and demonstrated a new approach for designing super-low ice adhesion surfaces (SLIAS). By introducing sub-structures into smooth polydimethylsiloxane (PDMS) coatings, the SLIAS reached an ultra-low ice adhesion of 5.7 kPa.[32] In general, extremely low elastic moduli are required to achieve significant icephobicity. Yet, these extremely soft surfaces are not mechanically robust.[31] Short lifespans of these materials can not be avoided. Extending the life-time of icephobic surfaces is, therefore, as critical as achieving ultralow ice adhesion strength for anti-icing.

In nature, living organisms can repair their physical damages to survive in harsh environments and prolong their longevity. Inspired by such functionality, a range of self-healing polymeric materials had been developed and applied to various fields for extending the life-span in applications.[33-36] Specially, intrinsically self-healing polymers possess dynamic bonds (hydrogen bonds,[35] metal-ligand coordination,[36-37] electrostatic interactions,[38] and so on) that are missing in conventional polymers. The self-healing ability results from the breaking and reforming of the dynamic bonds. When soft icephobic materials are endowed with such self-healing functionality, it can be expected that these materials will possess the ability of healing mechanical damages at both micro- and mesoscale in the icing and deicing cycles, and preventing the development of catastrophic damage. To the best of our knowledge, enabling autonomous self-healing property in icephobic materials has not been reported as a strategy of improved durability.

Herein, we designed a new icephobic material by integrating interpenetrating polymer network (IPN) into an autonomous self-healing elastomer for anti-icing purpose. We studied the creep behavior of the new self-healing icephobic material that was not covered in most relevant studies.[39] According to previous studies, the minimal shear stress (ice adhesion

strength, τ) to separate ice from a soft coating is given by $\propto (EG/t)^{1/2}$, where E is the elastic modulus, G is the surface energy and t is the thickness of the coating.[11, 29-30, 32] Low shear modulus and surface energy can lead to low ice adhesion strength. Therefore, we selected self-healing PDMS-based elastomer, Fe-Py-PDMS, as the matrix due to its low modulus and surface energy. The self-healing property in the selected PDMS-based elastomer has been reported in a former study.[36] The polymer chains in such self-healing elastomer are crosslinked by metal-ligand coordination bonds, which are relatively weaker than covalent bonds. As such, the elastomer can easily creep under load, resulting in the formation of surface texture, which can lead to high ice adhesion strength due to mechanical interlocking.[40-41] As illustrated in **Figure 1**, we further designed and integrated interpenetrating polymer networks (IPNs) into the elastomer for forming a new icephobic material. We introduced the commercial PDMS, Sylgard 184, into the material matrix to form integrated IPNs. The two parts in the material, self-healing elastomer crosslinked via metal-ligand coordination bonds and commercial PDMS crosslinked via covalent bonds, synergistically led self-healing property and enhanced creep resistance compared with the previous self-healing elastomer. The new icephobic material demonstrated durable icephobicity, namely achieving an ultralow ice adhesion strength of 6.0±0.9 kPa, and remaining at a very low value (around 12.2±3.7 kPa) after 50 icing/deicing cycles. Significantly, the material showed self-healing property before and after the deicing studies, which confirmed our new design for icephobic surface durability.

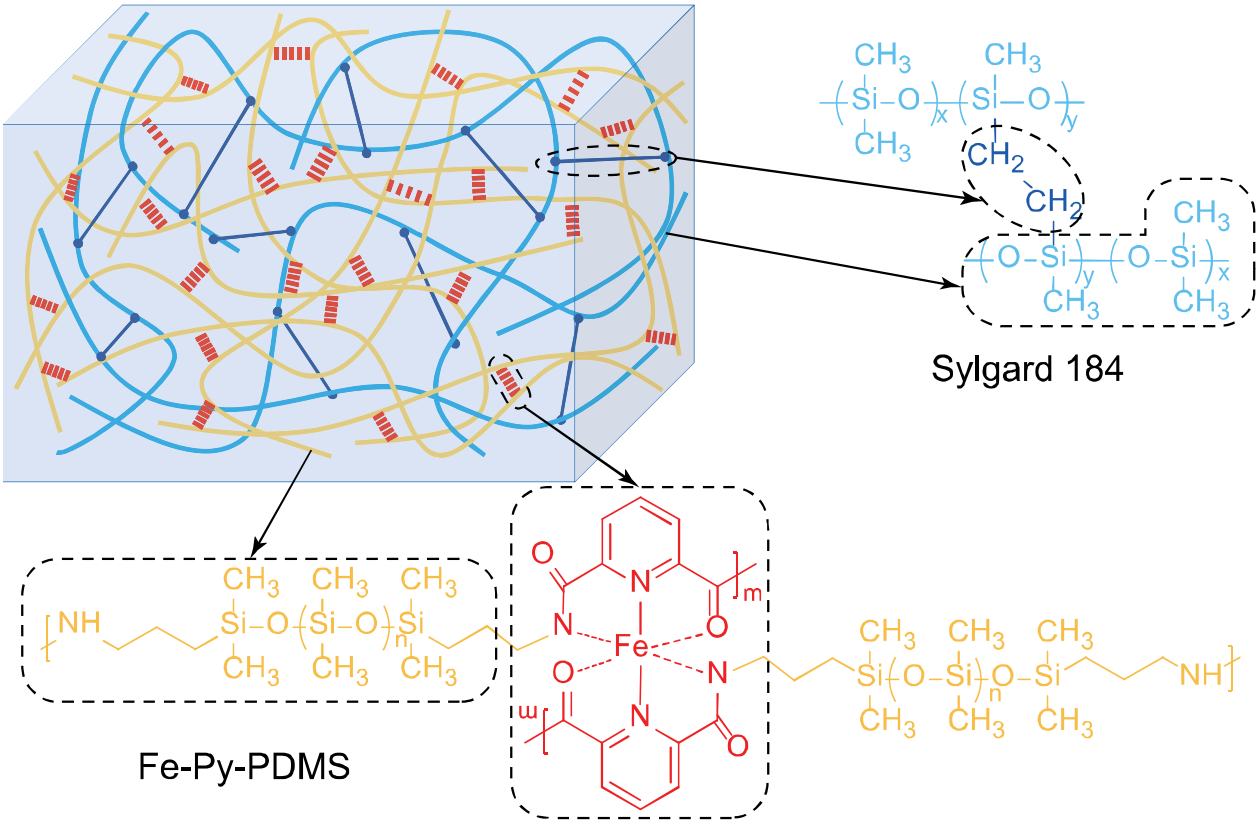

Figure 1 Scheme of the self-healing IPN elastomer consisting of Fe-Py-PDMS and Sylgard 184. Sylgard 184 is crosslinked via covalent bond, while Fe-Py-PDMS is crosslinked via metal-ligand coordination.

EXPERIMENTAL SECTION

Materials: Bis(3-aminopropyl) terminated poly(dimethylsiloxane) (H_2N-PDMS-NH_2, Mn = 5000) was provided by Gelest. Sylgard 184 kits were obtained from Dow Corning. The rest of reagents and solvents were purchased from Sigma-Aldrich. All chemicals were used as received without further purification.

Synthesis of Py-PDMS ligand: Py-PDMS ligand was synthesized according to a previous report, as shown in **Scheme S1** (Supporting Information).[36] A mixture of H_2N-PDMS-NH_2 (50 g) and anhydrous CH_2Cl_2 (80 mL) was placed into a 250 mL flask equipped

with a magnetic stirrer. Then triethylamine (3.5 mL) was added into the mixture at 0℃ under nitrogen protection and stirred for 2 hours. Afterwards, a solution of 2,6-pyridinedicarbonyl dichloride (2.0401 g, 10 mmol) in CH_2Cl_2 (20 mL) was added into the mixture dropwise and stirred at 0℃ for another 2 hours. The resulted mixture was then kept at room temperature and stirred for 2 days under nitrogen atmosphere. After the reaction, 60 mL methanol was poured into the concentrated mixture to quench the reaction and yield white precipitate-like viscous liquid. The mixture was settled for several hours, followed by decanting the upper clear solution. CH_2Cl_2 (20 mL) was then added to dissolve the product. The purification process was repeated three times. The obtained mixture was vacuum evaporated to remove the remaining solvent and triethylamine. The final Py-PDMS product was characterized by ^{1}H NMR and ^{13}C NMR.

Preparation of interpenetrating polymer network coatings: 20x μL (x=8, 7, 5 or 3) of $FeCl_3$ (100 mg/mL) solution in methanol was added to a mixed solution of Py-PDMS (0.1x g) and Sylgard 184 base (0.1y g, y=8-x) in CH2Cl2 (4 mL). The mixed solution was stirred for 1 day at room temperature and then concentrated to about 2 mL. Then Sylgard 184 curing agent (0.01y g, 97y μL) was added into the mixture, followed by vigorous stirring for 10 min. The concentrated solution was poured into a home-made mold, as shown in **Figure S1** (Supporting Information), where glass pieces were treated with oxygen plasma (Diener Electronics, Femto, 50% O_2 flow, 50% power) for 3 min before casting. After drying at room temperature for 2 days, the films were curing at 80 °C for another 10 h. The as-prepared coatings were termed x-y, where x:y is the weight ratio of Py-PDMS to Sylgard 184 base.

Characterization: Chemical structures of Py-PDMS and coatings were examined by nuclear magnetic resonance (NMR, Bruker Avance III 400 MHz), Raman spectroscopy

(Renishaw, InVia Reflex Spectrometer System), and FT-IR spectroscopy (Thermo Nicolet Nexus FT-IR spectrometer). Scanning electron microscopy (SEM) and energy dispersive X-ray spectroscopy (EDX) were carried out in the field emmision scanning electron microscope (FEI APREO SEM) equipped with an EDX detector (Oxford X-Max). All samples were sputter-coated with a 10 nm platinum/palladium layer. The surface morphology of the coatings was recorded by Atomic Force Microscopy (AFM, Veeco Metrology) using PeakForce Quantitative NanoMechanics mode. Digital photos of coatings were taken by a Canon EOS 800D camera. Optical microscopy images of the self-healing process were captured by microscope with an integrated camera (Carl Zeiss, Primo star). Quasi-static nanoindentation tests were conducted in a TriboIndenter® 950 (Hysitron, Inc.) by using a cylindrical diamond flat punch with 53.70±0.06 μm diameter. Thicknesses of the coatings were measured by an absolute digimatic indicator (Mitutoyo, ID-C112GB). Ice adhesion strength was measured by an Instron machine (Model 5944) equipped with home-built cooling system and chamber, as depicted in previous reports.[32, 42] A polypropylene centrifuge tube mold with a 1 mm thick wall and a 27.5 mm inner diameter was placed onto the coatings acting as an ice mold, followed by the pressure of a 200 g metal cylinder to avoid water leakage. Then, 5 mL deionized water was syringed into the mold, followed by transfer to in a freezer at -18 °C for more than 2 hours to ensure complete freezing. Before test, the samples were transferred from the freezer to the cooling chamber and stabilized at -18 °C for 30 min. During ice adhesion tests, a force probe with 5 mm diameter propelled the tube-encased ice columns at a velocity of 0.01 mm s^{-1}, and the probe was located close to the tested coating surface (less than 1 mm) to minimize the torque on the ice cylinder. The loading curve was recorded, and the peak value of the shear force was divided by contact area to obtain the ice adhesion strength.

RESULTS AND DISCUSSION

Fabrication and characterization of self-healing IPN elastomer. Organic ligands, 2,6-pydinedicarboxamide groups, were introduced to the PDMS backbone by condensation reactions between 2,6-pyridinedicarbonyl dichloride and bis(3-aminopropyl)-terminated PDMS (H_2N-PDMS-NH_2) to give pydinedicarboxamide-containing PDMS (Py-PDMS) according to a previous study.[36] More details are given in the Experimental section and Scheme S1 in the Supporting Information. The ^{1}H NMR and ^{13}C NMR spectra of Py-PDMS confirmed the expected chemical structure as shown in **Figure S2** and **Figure S3** in the Supporting Information. We then mixed different weight ratio (8:0, 7:1, 5:3, 3:5, and 0:8) of Py-PDMS and Sylgard 184 base together, followed by adding Fe(III) chloride and Sylgard 184 curing agent separately to obtain the IPN elastomer (**Figure 1**). As-prepared elastomer is termed x-y in the following text, where x:y is the weight ratio of Py-PDMS to Sylgard 184 base. 8-0 and 0-8 are also named as Fe-Py-PDMS and Sylgard 184, respectively. We used Raman spectra to characterize the formation of the polymer network, as shown in **Figure 2a**. Compared with Py-PDMS and 0-8, a new peak at around 330 cm^{-1} referring to the Fe-N coordination is observed in the Raman spectra of 8-0, 7-1 and 5-3, indicating the successful formation of crosslinked Fe-Py-PDMS network. One can see in **Figure 2a** that the percentage of Fe-N coordination increased with the weight ratio of Py-PDMS to Sylgard 184 base. Furthermore, FT-IR spectra shown in **Figure 2b** confirm wavenumber shifts of amide band I and amide band II from 1685 cm^{-1} (black dash line) to 1636 cm^{-1} (black solid line) and from 1536 cm^{-1} (red dash line) to 1541 cm^{-1} (red solid line), respectively, which were in good agreement with former results of the formation of metal-ligand coordination complex.[36]

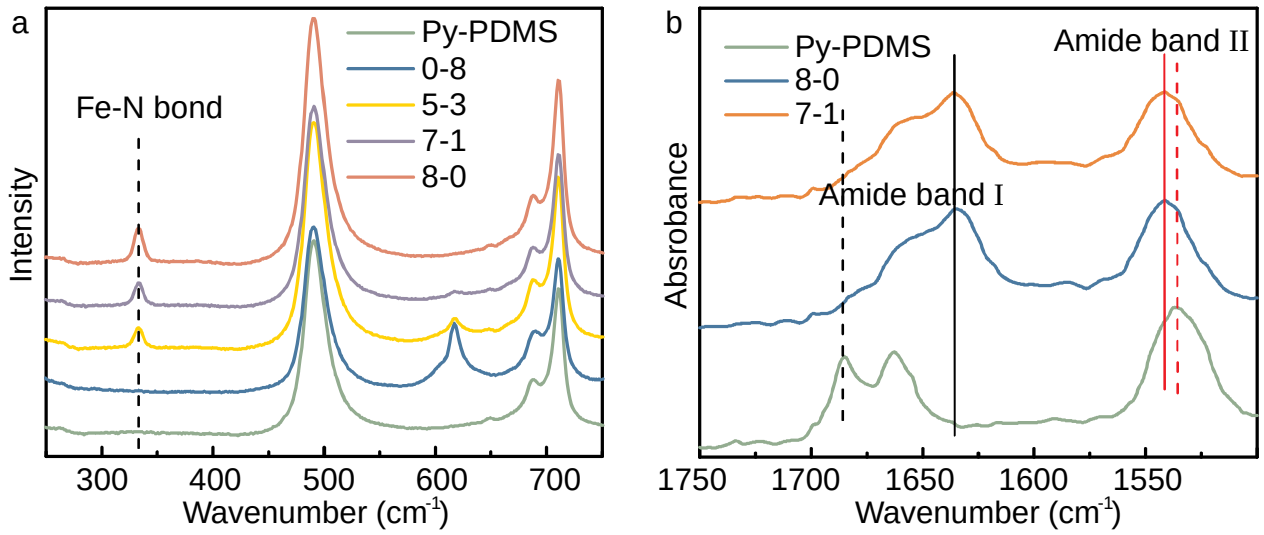

Figure 2 (a) Raman spectra of Py-PDMS and samples with weight ratios of 0-8 (pure Sylgard 184), 5-3, 7-1 and 8-0 (pure Fe-Py-PDMS) of Sylgard 184 and Fe-Py-PDMS in the range of 250-750 cm-1. (b) FT-IR spectra of Py-PDMS and samples with 8-0 and 7-1 weight ratios of Sylgard 184 and Fe-Py-PDMS in the range of 1750-1500 cm^{-1}.

Surface Morphology. Owing to the Fe(III), the self-healing elastomer was orangered but transparent, as an example elastomer 7-1 shown in **Figure 3a**. The surfaces of all the samples were smooth and compact as confirmed by scanning electron microscopy (SEM) characterization shown in **Figure 3b**. Such optical transparency and smooth surface evidence that the material was homogeneous and had no phase separation, which is reasonable considering that the two parts of the network, Sylgard 184 and Fe-Py-PDMS, have the same PDMS backbone. Energy dispersive X-ray (EDX) analyses in **Figure 3c, Figure S4** and **Figure S5** in the Supporting Information, further confirmed the homogeneous distribution of the two components. As depicted in **Figure 3c**, all elements of interest (C, O, N, Si, Fe, Cl) along the white line in **Figure 3b** featured uniform distributions by the EDX line scan, as well as EDX area scans shown in **Figure S4**. The surface topography of the coatings characterized by atomic force microscopy (AFM) were

shown in **Figure 3d**. All surfaces had a root-mean-squared roughness below 10 nm (see roughness data in **Table S1**, Supporting Information).

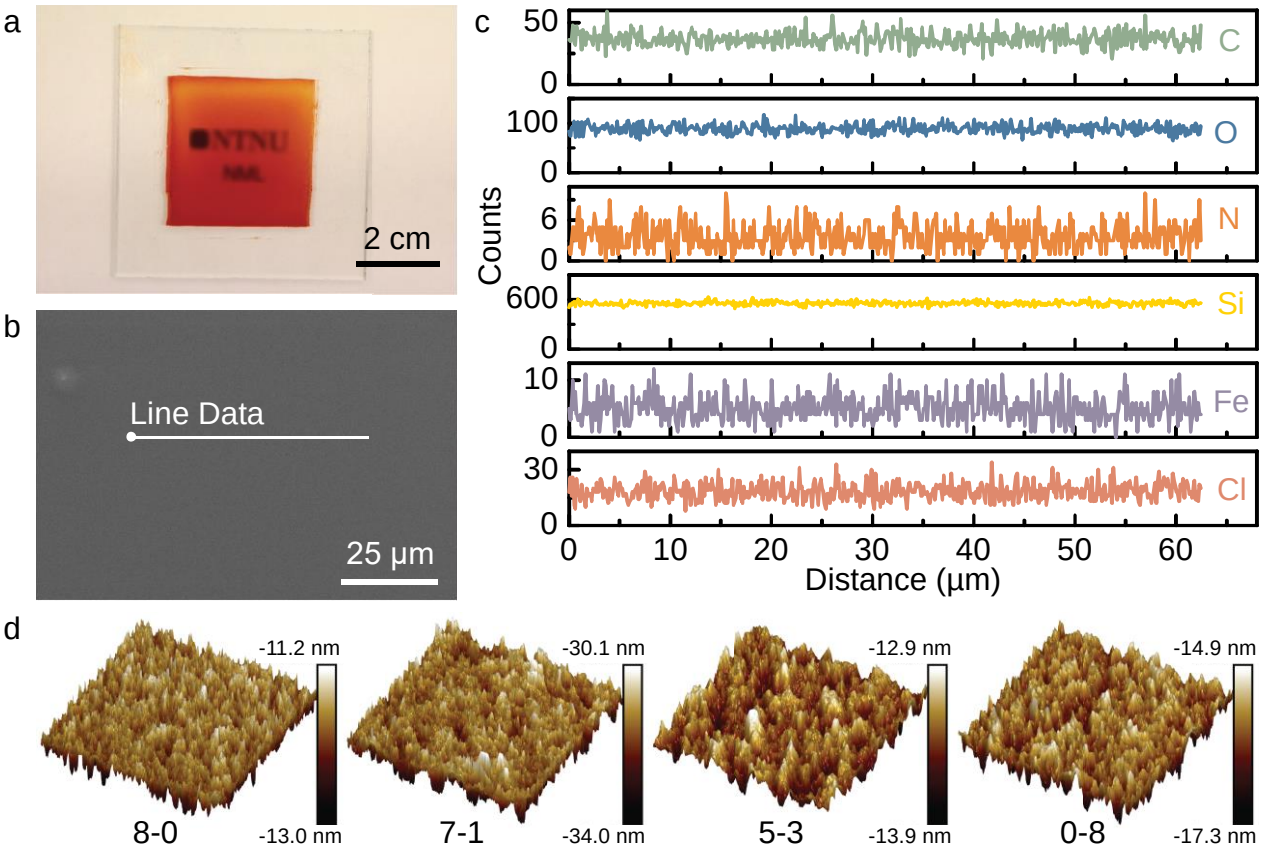

Figure 3 (a) A digital photo of 7-1 demonstrates the same orange red color and transparency of all the self-healing elastomer samples. (b) SEM image of 7-1 shows the smooth and compact surface, as an example of all the samples. (c) EDX line scans of elements of interest (C, O, N, Si, Fe, Cl), exemplified by 7-1. (d) AFM 3D height images of 8-0, 7-1, 5-3 and 0-8 with scan size 500×500 nm^2.

Mechanical properties. As discussed above, the elastic modulus of the coating is the key to the ice adhesion strength of soft coatings. To investigate the mechanical properties of the as-prepared coatings, quasi-static nanoindentation tests had been carried out by using cylindrical flat punch with 53.70±0.06 μm diameter. The samples were rapidly loaded to the maximum load (P_{max}) in 1 second, and then held in the P_{max} for 10 seconds, followed

by unloading in 1 second. The P_{max} for 8-0, 5-3, 0-8 is 50 μN. The P_{max} for 7-1 was set to 10 μN since the 7-1 was too soft to hold the load of 50 μN in the limitation of displacement (5 μm). The resulting load-displacement curves are shown in **Figure 4a**. The unloading stiffness *S* of the coatings can be obtained by linear fitting the slope of the initial portion of the unloading curve, as illustrated by the black fitting line in **Figure 4a**. The reduced modulus of the sample is calculated as: $E_r = S/D$ where *D* is the diameter of the cylindrical flat punch.[43] The obtained unloading stiffness and the corresponding reduce modulus are given in **Table S1** in the Supporting Information and **Figure 4b**, respectively. The pristine elastomers 8-0 (Fe-Py-PDMS) and 0-8 (Sylgard 184) possess reduced moduli of 0.92±0.01 MPa and 1.85±0.01 MPa, respectively, while the IPN elastomers 7-1 and 5-3 showed reduced moduli of 0.29±0.01 MPa and 0.47±0.03 MPa, respectively. Young's modulus of the materials can also be estimated, since it is related to the measured reduced modulus, as: $1/E_{\mathrm{r}} = (1-v^2)/E + \left(1-v_{\mathrm{tip}}^2\right)/E_{\mathrm{tip}}$, where *v* and v_{tip} are Poisson's ratio of material and diamond indenter respectively, *E* and E_{tip} are Young's modulus of material and diamond indenter respectively. Here, the *v* for all samples was assumed to be the same and equal to 0.5, and $v_{\mathrm{tip}} = 0.07$, $E_{\mathrm{tip}} = 1140\ GPa$.[43-44] Since $E_{\mathrm{tip}} \gg E$, the second term of the equation is negligible. Hence, Young's modulus of the samples is approximated to: $E = E_{\mathrm{r}}(1-v^2) = 0.75E_{\mathrm{r}}$. The estimated Young's modulus of the samples is shown in **Table S1** (Supporting information). The decrease of modulus in the IPN elastomers can be ascribed to the plastication effect of Sylgard 184 on Fe-Py-PDMS.

The creep behaviors of the coatings can be obtained from the holding segment in the load-displacement curve. As shown in **Figure 4a**, a large creep segment appeared in the 8-0 (Fe-Py-PDMS) loading curve, which was not observed in the 0-8 (Sylgard 184) curve.

Compared to 8-0 (Fe-Py-PDMS), the 5-3 (IPN elastomer) showed much smaller creep displacement due to the existence of Sylgard 184. In order to visualize the creep behaviors of the coatings, we placed a polypropylene tube with an inner diameter of 27.5 mm and a wall of 1 mm thick on the coating surface, followed by the pressure of a 200 g metal cylinder for 24 h, as shown in **Figure S6** in the Supporting Information. The comparison of samples before and after the test is shown in **Figure 4c** and **Figure 4d**, respectively. Distinct indentation was found on the surface of 8-0 after the test, while only slight and negligible indentation could be observed on the other surfaces. The creep deformation of the coatings can be attributed to the rupture of the metal-ligand coordination complex and the slippage of polymeric chains under force, and the rearrangement of metal-ligand coordination complex, as schematically illustration in **Figure 5**. The rupture of metal-ligand coordination can lead to slippage and reptation of polymeric chains, which can further lead to formation of the new coordination sites and result in permanent deformation. These results suggested that the creep resistance of IPN elastomers (7-1 and 5-3) were much higher than that of 8-0, owing to the presence of covalent crosslinking network (Sylgard 184). The Sylgard 184 in the IPN elastomer (7-1 and 5-3) served as a scaffold efficiently suppressing the mobility of the polymeric chains and restrained the rupture of the metal-ligand coordination complex. Thus, the overall result of which was the expected enhanced creep resistance.

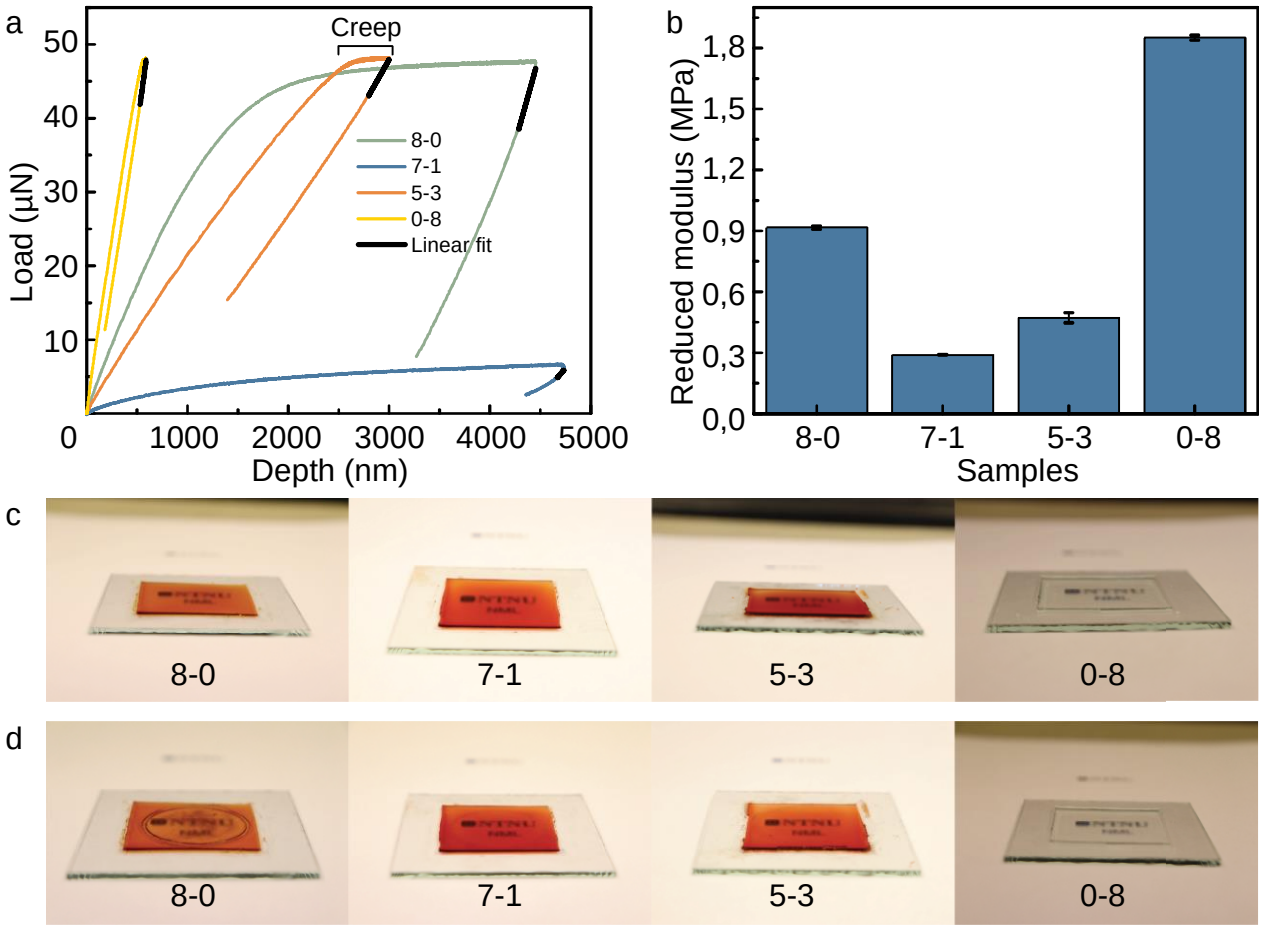

Figure 4 (a) The load-displacement curves of 8-0, 7-1, 5-3, and 0-8 from flat punch nanoindentation tests. (b) Reduced modulus of the samples obtained from the nanoindentation tests. (c) Digital photos of 8-0, 7-1, 5-3 and 0-8 before creep visualized test. (d) Digital photos of 8-0, 7-1, 5-3 and 0-8 after creep visualized test.

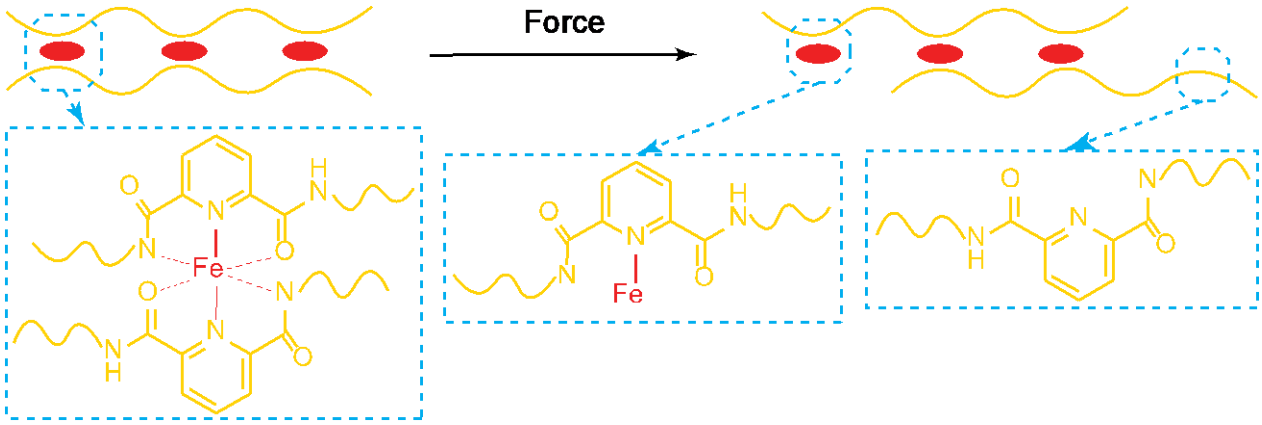

Figure 5 Schematic metal-ligand coordination complex rupture and polymeric chains slippage under force, and the rearrangement of metal-ligand coordination complex.

Self-healing properties. The self-healing process of the IPN coatings recorded by using optical microscopy is shown in **Figure 6**. The coatings were first cut by a scalpel, and subsequently set to self-heal at room temperature without any treatment. From the images in **Figure 6**, the fresh cut can be observed clearly for all elastomers. The scars faded away on 8-0 and 7-1 elastomers after healing in 24 to 48 hours while it was still visible on 5-3 after 96 hours. The self-healing properties can be attributed to the presence of reversible metal-ligand coordination bonds as well as the high mobility of the polymeric chain.[36] During the self-healing process, the flexible polymeric chain allows the ligands and metal ions to migrate together easily, followed by the reconstruction of coordination complexes. Combined with the nanoindentation results, it is clear that the presence of covalent crosslinked network in the as-prepared self-healing elastomer can enhance creep resistance, but at the same time suppress self-healing rate. Upon addition of a covalent crosslinked network, the mobility of the polymeric chain is expected to be restricted, which leads to a better creep resistance and hindrance of the contacts between metal ions and ligands. As a result, there is a trade-off between creep resistance and self-healing rate in as-prepared IPN elastomer. Future work will be dedicated to overcoming this trade-off.

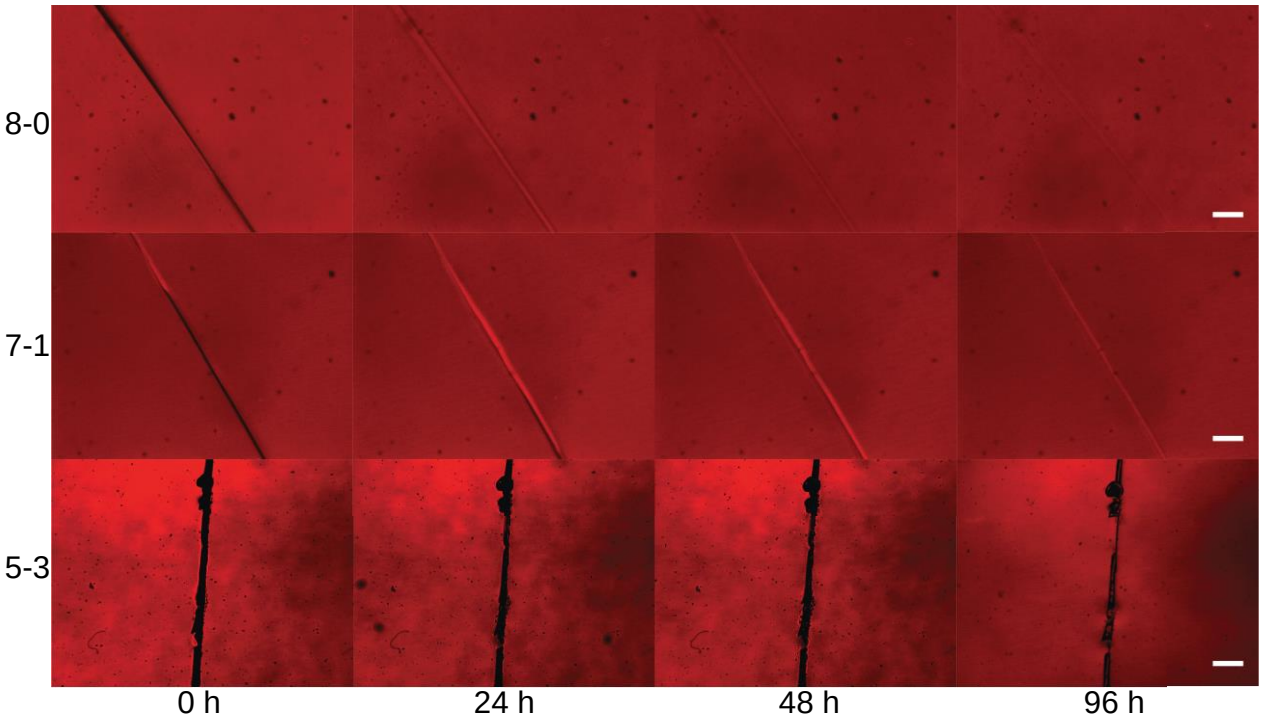

Figure 6 Optical microscopy image showing the self-healing process of 8-0, 7-1 and 5-3. Scale bar: 200 μm.

Anti-icing properties. We evaluated ice adhesion strength on our samples in a vertical shear mode at -18 °C as depicted in previous studies.[32, 42] Since the ice adhesion strength of soft coatings is related to their thickness,[22] we measured the thickness of our coatings before the ice adhesion test. All coatings showed thicknesses in the range between 300 and 342 μm (see details in **Table S1**, Supporting Information). **Figure 7a** shows the ice adhesion strength of the as-prepared samples, 0-8 (Sylgard 184 coating) had an ice adhesion strength of 169.6±3.3 kPa, close to the reported value for PDMS in the same thickness range.[22] The ice adhesion strength of 8-0 (Fe-Py-PDMS) coating was found to be 63.9±2.2 kPa, showing a ~62% reduction compared to the Sylgard 184 coating. More significantly, the as-prepared IPN elastomers 7-1 and 5-3 showed surprisingly lower ice adhesion strength of 6.0±0.9 kPa and 17.2±3.0 kPa, respectively. The ice adhesion strength of the as-prepared samples

followed the same trend as the reduced modulus and unloading stiffness. It is noteworthy that the ice adhesion strength of 6.0±0.9 kPa for 7-1 is below the critical value (⩽12 kPa) that ice can be removed by wind shear or solely under its own weight.[31] The ultralow reduced modulus and unloading stiffness (rigidity) of the IPN elastomer facilitate the formation of cavities at the ice- coating interface, and the formed voids can serve as crack initiators and promote the separation of ice from the coating.[29] It should be noted that interfacial slippage might occur at the ice-coating interface due to the effect of unreacted polymeric chains in the elastomer, which is also in favor of the detachment.[11, 45]

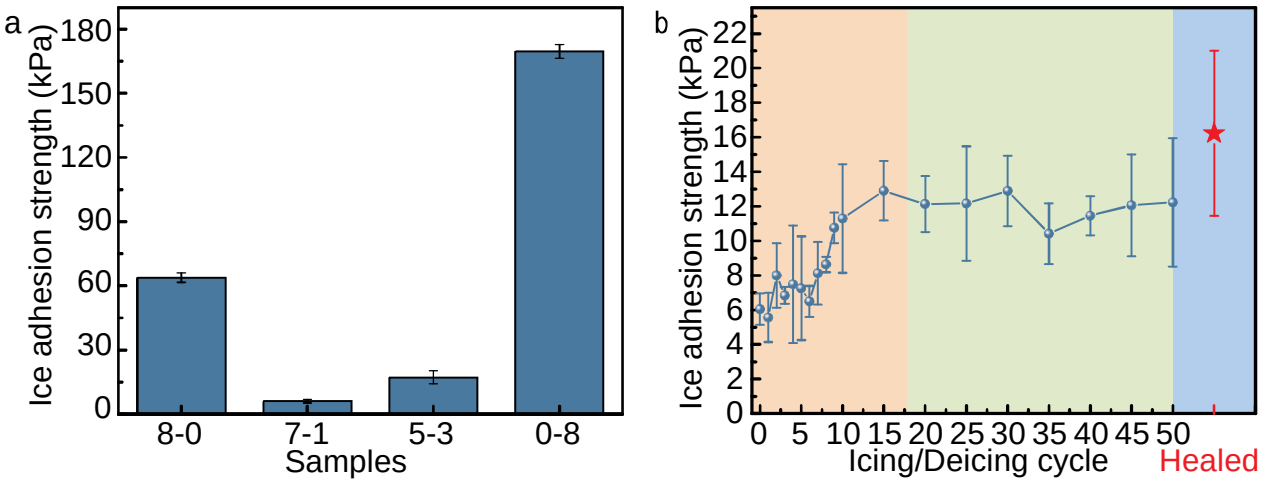

Figure 7 (a) Ice adhesion strengths of 8-0 (Fe-Py-PDMS), 7-1, 5-3 and 0-8 (Sylgard 184 coating). (b) Ice adhesion strengths of 7-1 during icing/deicing cycles and after self-healed.

While ice adhesion strength is of great importance for icephobic materials, their durability is also crucial to the outdoor applications. We thus performed cyclic icing and deicing tests on the 7-1 elastomer to evaluate the durability of as-prepared materials. As shown in **Figure 7b**, the ice adhesion strength of the 7-1 elastomer increased during the initial 15 cycles, mostly due to the removal of unreacted polymeric chains during ice detaching. Subsequently, ice adhesion strength kept steady at around 12.2 kPa in 50 icing/deicing cycles. In addition, the coating after 50 icing/deicing cycles still showed self-healing ability,

as shown in **Figure S7** (Supporting Information). Moreover, we cut a cross throughout the coating surface, followed by self-healing for 4 days, and then tested the ice adhesion strength of the healed surface. As shown in **Figure 7b**, the healed surface shows slight increase of ice adhesion strength. Adhesive failure instead of cohesive failure occurred during the separation of ice and coating in all icing and deicing cycles. Furthermore, the self-healing property of the coating can prevent severe mechanical damage and ensure the integrity of the coating surface to survive through the deicing process, which enables the longevity of the icephobicity.

CONCLUSIONS

In summary, this work had designed and fabricated a new icephobic material with ultralow ice adhesion strength by combining robust IPN and effective autonomous self-healing elastomer. Fe-Py-PDMS with dynamic metal-ligand coordination bonds and commercial PDMS Sylgard 184 were chosen and mixed to form interpenetrating polymer networks (IPN). Such IPN-contained elastomer demonstrated good creep resistance and great potential in anti-icing applications with an ultralow ice adhesion strength of 6.0±0.9 kPa. Most importantly, the new icephobic material displayed excellent durability and maintained low ice adhesion strength (around 12.2 kPa) after 50 icing/deicing cycles. This study also looked into the creep behavior of the self-healing elastomer, and detailed the trade-off of creep resistance and self-healing rate. This work brings a new strategy, namely self-healing for longevity, into the design of durable icephobic materials, and in a broad range of anti-adhesive applications.

ASSOCIATED CONTENT

Supporting Information. The Supporting Information is available free of charge via the Internet at http://pubs.acs.org. Synthesis route; schematic of home-made mold for coating preparation; NMR spectrum; EDX area scans and spectrum; schematic of creep visualization test and self-healing process after icing/deicing cycles are given in the Supporting Information.

AUTHOR INFORMATION

Corresponding Author

*E-mail: jianying.he@ntnu.no; zhiliang.zhang@ntnu.no

ACKNOWLEDGMENT

The Research Council of Norway is acknowledged for the support to the PETROMAKS2 Project Durable Arctic Icephobic Materials (Project No. 255507) and for the support to the Norwegian Micro- and Nano-Fabrication Facility, NorFab, project number 245963. The authors thank Jing Deng at Department of Chemical Engineering, Norwegian University of Science and Technology for helping on FT-IR spectra.

REFERENCES

1. Kreder, M. J.; Alvarenga, J.; Kim, P.; Aizenberg, J., Design of anti-icing surfaces: smooth, textured or slippery? *Nat. Rev. Mater.* **2016,** *1* (1), 15003.

2. Chen, D.; Gelenter, M. D.; Hong, M.; Cohen, R. E.; McKinley, G. H., Icephobic surfaces induced by interfacial non-frozen water. *ACS Appl. Mater. Interfaces* **2017**, *9* (4), 4202-4214.

3. Wang, L.; Gong, Q.; Zhan, S.; Jiang, L.; Zheng, Y., Robust Anti-Icing Performance of a Flexible Superhydrophobic Surface. *Adv. Mater.* **2016,** *28* (35), 7729-7735.

4. Schutzius, T. M.; Jung, S.; Maitra, T.; Eberle, P.; Antonini, C.; Stamatopoulos, C.; Poulikakos, D., Physics of icing and rational design of surfaces with extraordinary icephobicity. *Langmuir* **2015,** *31* (17), 4807-4821.

5. Maitra, T.; Tiwari, M. K.; Antonini, C.; Schoch, P.; Jung, S.; Eberle, P.; Poulikakos, D., On the nanoengineering of superhydrophobic and impalement resistant surface textures below the freezing temperature. *Nano Lett.* **2014,** *14* (1), 172-182.

6. Momen, G.; Jafari, R.; Farzaneh, M., Ice repellency behaviour of superhydrophobic surfaces: Effects of atmospheric icing conditions and surface roughness. *Appl. Surf. Sci.* **2015,** *349* (0), 211-218.

7. Yang, H.; Ma, C.; Li, K.; Liu, K.; Loznik, M.; Teeuwen, R.; van Hest, J. C.; Zhou, X.; Herrmann, A.; Wang, J., Tuning Ice Nucleation with Supercharged Polypeptides. *Adv. Mater.* **2016,** *28* (25), 5008-5012.

8. He, Z.; Xie, W. J.; Liu, Z.; Liu, G.; Wang, Z.; Gao, Y. Q.; Wang, J., Tuning ice nucleation with counterions on polyelectrolyte brush surfaces. *Sci. Adv.* **2016,** *2* (6), e1600345.

9. He, Z.; Zheng, L.; Liu, Z.; Jin, S.; Li, C.; Wang, J., Inhibition of Heterogeneous Ice Nucleation by Bioinspired Coatings of Polyampholytes. *ACS Appl. Mater. Interfaces* **2017,** *9* (35), 30092-30099.

10. Sojoudi, H.; Wang, M.; Boscher, N. D.; McKinley, G. H.; Gleason, K. K., Durable and scalable icephobic surfaces: similarities and distinctions from superhydrophobic surfaces. *Soft Matter* **2016,** *12* (7), 1938-1963.

11. Golovin, K.; Kobaku, S. P.; Lee, D. H.; DiLoreto, E. T.; Mabry, J. M.; Tuteja, A., Designing durable icephobic surfaces. *Sci. Adv.* **2016,** *2* (3), e1501496.

12. Ling, E. J.; Uong, V.; Renault-Crispo, J. S.; Kietzig, A. M.; Servio, P., Reducing Ice Adhesion on Nonsmooth Metallic Surfaces: Wettability and Topography Effects. *ACS Appl. Mater. Interfaces* **2016,** *8* (13), 8789-8800.

13. Bengaluru Subramanyam, S.; Kondrashov, V.; Ruhe, J.; Varanasi, K. K., Low Ice Adhesion on Nano-Textured Superhydrophobic Surfaces under Supersaturated Conditions. *ACS Appl. Mater. Interfaces* **2016,** *8* (20), 12583-12587.

14. Boinovich, L. B.; Emelyanenko, A. M.; Ivanov, V. K.; Pashinin, A. S., Durable icephobic coating for stainless steel. *ACS Appl. Mater. Interfaces* **2013,** *5* (7), 2549-2554.

15. Guerin, F.; Laforte, C.; Farinas, M.-I.; Perron, J., Analytical model based on experimental data of centrifuge ice adhesion tests with different substrates. *Cold Reg. Sci. Technol.* **2016,** *121*, 93-99.

16. Dou, R.; Chen, J.; Zhang, Y.; Wang, X.; Cui, D.; Song, Y.; Jiang, L.; Wang, J., Anti-icing coating with an aqueous lubricating layer. *ACS Appl. Mater. Interfaces* **2014,** *6* (10), 6998-7003.

17. Li, Y.; Luo, C.; Li, X.; Zhang, K.; Zhao, Y.; Zhu, K.; Yuan, X., Submicron/nano-structured icephobic surfaces made from fluorinated polymethylsiloxane and octavinyl-POSS. *Appl. Surf. Sci.* **2016,** *360*, 113-120.

18. Meuler, A. J.; Smith, J. D.; Varanasi, K. K.; Mabry, J. M.; McKinley, G. H.; Cohen, R. E., Relationships between Water Wettability and Ice Adhesion. *ACS Appl. Mater. Interfaces* **2010,** *2* (11), 3100-3110.

19. Hejazi, V.; Sobolev, K.; Nosonovsky, M., From superhydrophobicity to icephobicity: Forces and interaction analysis. *Sci. Rep.* **2013,** *3, 2194*.

20. Sojoudi, H.; McKinley, G. H.; Gleason, K. K., Linker-free grafting of fluorinated polymeric cross-linked network bilayers for durable reduction of ice adhesion. *Mater. Horiz.* **2015,** *2* (1), 91-99.

21. Kulinich, S. A.; Honda, M.; Zhu, A. L.; Rozhin, A. G.; Du, X. W., The icephobic performance of alkyl-grafted aluminum surfaces. *Soft Matter* **2015,** *11* (5), 856-861.

22. Wang, C.; Fuller, T.; Zhang, W.; Wynne, K. J., Thickness dependence of ice removal stress for a polydimethylsiloxane nanocomposite: Sylgard 184. *Langmuir* **2014,** *30* (43), 12819-12826.

23. Wong, T.-S.; Kang, S. H.; Tang, S. K. Y.; Smythe, E. J.; Hatton, B. D.; Grinthal, A.; Aizenberg, J., Bioinspired Self-Repairing Slippery Surfaces with Pressure-Stable Omniphobicity. *Nature* **2011,** *477* (7365), 443-447.

24. Kim, P.; Wong, T.-S.; Alvarenga, J.; Kreder, M. J.; Adorno-Martinez, W. E.; Aizenberg, J., Liquid-infused nanostructured surfaces with extreme anti-ice and anti-frost performance. *ACS Nano* **2012,** *6* (8), 6569-6577.

25. Nosonovsky, M.; Hejazi, V., Why superhydrophobic surfaces are not always icephobic. *ACS Nano* **2012,** *6* (10), 8488-8491.

26. Wang, Y.; Yao, X.; Chen, J.; He, Z.; Liu, J.; Li, Q.; Wang, J.; Jiang, L., Organogel as durable anti-icing coatings. *Sci. China Mater.* **2015,** *58* (7), 559-565.

27. Urata, C.; Dunderdale, G. J.; England, M. W.; Hozumi, A., Self-lubricating organogels (SLUGs) with exceptional syneresis-induced anti-sticking properties against viscous emulsions and ices. *J. Mater. Chem. A* **2015,** *3* (24), 12626-12630.

28. Wang, Y.; Yao, X.; Wu, S.; Li, Q.; Lv, J.; Wang, J.; Jiang, L., Bioinspired Solid Organogel Materials with a Regenerable Sacrificial Alkane Surface Layer. *Adv. Mater.* **2017,** *29* (26), 170086.

29. Beemer, D. L.; Wang, W.; Kota, A. K., Durable gels with ultra-low adhesion to ice. *J. Mater. Chem. A* **2016,** *4* (47), 18253-18258.

30. Chaudhury, M. K.; Kim, K. H., Shear-induced adhesive failure of a rigid slab in contact with a thin confined film. *Eur. Phys. J. E: Soft Matter Biol. Phys.* **2007,** *23* (2), 175-183.

31. Golovin, K.; Tuteja, A., A predictive framework for the design and fabrication of icephobic polymers. *Sci. Adv.* **2017,** *3* (9), e1701617.

32. He, Z.; Xiao, S.; Gao, H.; He, J.; Zhang, Z., Multiscale crack initiator promoted super-low ice adhesion surfaces. *Soft Matter* **2017,** *13* (37), 6562-6568.

33. Huynh, T. P.; Sonar, P.; Haick, H., Advanced Materials for Use in Soft Self-Healing Devices. *Adv. Mater.* **2017,** *29* (19), 1604973.

34. Jin, B.; Liu, M.; Zhang, Q.; Zhan, X.; Chen, F., Silicone Oil Swelling Slippery Surfaces Based on Mussel-Inspired Magnetic Nanoparticles with Multiple Self-Healing Mechanisms. *Langmuir* **2017,** *33* (39), 10340-10350.

35. Cordier, P.; Tournilhac, F.; Soulie-Ziakovic, C.; Leibler, L., Self-healing and thermoreversible rubber from supramolecular assembly. *Nature* **2008,** *451* (7181), 977-980.

36. Li, C. H.; Wang, C.; Keplinger, C.; Zuo, J. L.; Jin, L.; Sun, Y.; Zheng, P.; Cao, Y.; Lissel, F.; Linder, C.; You, X. Z.; Bao, Z., A highly stretchable autonomous self-healing elastomer. *Nat. Chem.* **2016,** *8* (6), 618-624.

37. Liu, J.; Liu, J.; Wang, S.; Huang, J.; Wu, S.; Tang, Z.; Guo, B.; Zhang, L., An advanced elastomer with an unprecedented combination of excellent mechanical properties and high self-healing capability. *J. Mater. Chem. A* **2017,** *5* (48), 25660-25671.

38. Odent, J.; Raquez, J. M.; Dubois, P.; Giannelis, E. P., Ultra-stretchable ionic nanocomposites: from dynamic bonding to multi-responsive behavior. *J. Mater. Chem. A* **2017,** *5* (26), 13357-13363.

39. Creton, C., 50th Anniversary Perspective: Networks and Gels: Soft but Dynamic and Tough. *Macromolecules* **2017,** *50* (21), 8297-8316.

40. Liu, B.; Zhang, K.; Tao, C.; Zhao, Y.; Li, X.; Zhu, K.; Yuan, X., Strategies for anti-icing: low surface energy or liquid-infused? *RSC Adv.* **2016,** *6* (74), 70251-70260.

41. Chen, J.; Liu, J.; He, M.; Li, K.; Cui, D.; Zhang, Q.; Zeng, X.; Zhang, Y.; Wang, J.; Song, Y., Superhydrophobic surfaces cannot reduce ice adhesion. *Appl. Phys. Lett.* **2012,** *101* (11), 111603.

42. He, Z.; Vagenes, E. T.; Delabahan, C.; He, J.; Zhang, Z., Room Temperature Characteristics of Polymer-Based Low Ice Adhesion Surfaces. *Sci. Rep.* **2017,** *7,* 42181.

43. Wang, Z. X.; Volinsky, A. A.; Gallant, N. D., Nanoindentation Study of Polydimethylsiloxane Elastic Modulus Using Berkovich and Flat Punch Tips. *J. Appl. Polym. Sci.* **2015,** *132* (5), 41384.

44. Johnston, I. D.; McCluskey, D. K.; Tan, C. K. L.; Tracey, M. C., Mechanical characterization of bulk Sylgard 184 for microfluidics and microengineering. *J. Micromech. Microeng.* **2014,** *24* (3), 035017.

45. Xue, L.; Pham, J. T.; Iturri, J.; Del Campo, A., Stick-Slip Friction of PDMS Surfaces for Bioinspired Adhesives. *Langmuir* **2016,** *32* (10), 2428-2435.

Table of Contents